

ACCEPTED MANUSCRIPT • OPEN ACCESS

Tin Anode for High-Energy-Density Na-Ion Batteries

To cite this article before publication: Sihvun Kim et al 2025 J. Electrochem. Soc. in press https://doi.org/10.1149/1945-7111/ae0fc4

Manuscript version: Accepted Manuscript

Accepted Manuscript is "the version of the article accepted for publication including all changes made as a result of the peer review process, and which may also include the addition to the article by IOP Publishing of a header, an article ID, a cover sheet and/or an 'Accepted Manuscript' watermark, but excluding any other editing, typesetting or other changes made by IOP Publishing and/or its licensors"

This Accepted Manuscript is © 2025 The Author(s). Published on behalf of The Electrochemical Society by IOP Publishing Limited.

As the Version of Record of this article is going to be/has been published on a gold open access basis under a CC 4.0 licence, this Accepted Manuscript is available for reuse under the applicable CC licence immediately.

Everyone is permitted to use all or part of the original content in this article, provided that they adhere to all the terms of the applicable licence referred to in the article – either https://creativecommons.org/licenses/by/4.0/ or https://creativecommons.org/licenses/by/-nc-nd/4.0/

Although reasonable endeavours have been taken to obtain all necessary permissions from third parties to include their copyrighted content within this article, their full citation and copyright line may not be present in this Accepted Manuscript version. Before using any content from this article, please refer to the Version of Record on IOPscience once published for full citation and copyright details, as permissions may be required. All third party content is fully copyright protected and is not published on a gold open access basis under a CC licence, unless that is specifically stated in the figure caption in the Version of Record.

View the article online for updates and enhancements.

Tin Anode for High-Energy-Density Na-Ion Batteries

Journal:	Journal of The Electrochemical Society		
Manuscript ID	JES-115076.R1		
Manuscript Type:	Research Paper		
Date Submitted by the Author:	26-Sep-2025		
Complete List of Authors:	Kim, Sihyun; University of California San Diego Tang, Wei; University of California San Diego Lee, Dong Ju; University of California San Diego Wu, Junlin; University of California San Diego Jeon, Yuju; University of California San Diego, Aiiso Yufeng Li Department of Chemical and Nano Engineering Lu, Bingyu; Unigrid Battery Ham, So Yeon; Unigrid Battery Le, Viet; Unigrid Battery Ly, Layheack; Unigrid Battery Owens, Maria; Unigrid Battery Wu, Erik; Unigrid Battery Tan, Darran; Unigrid, Chen, Zheng; UC San Diego,		
Keywords:	Batteries, Electrochemical Engineering, Energy Storage, Sodium-ion battery, Tin anode		



Tin Anode for High-Energy-Density Na-Ion Batteries

Sihyun Kim,^{1,=} Wei Tang,^{1,=} Dong Ju Lee,¹ Junlin Wu,² Yuju Jeon,¹ Bingyu Lu,³ So-Yeon Ham,³ Viet Le,³ Layheack Ly,³ Maria L. Owens,³ Erik A. Wu,³ Darren H. S. Tan,³ and Zheng Chen^{1,2,4,2}

¹Aiiso Yufeng Li Department of Chemical and Nano Engineering, University of California, San Diego, La Jolla, California 92093, United States

²Program of Materials Science, University of California, San Diego, La Jolla, California 92093, USA

³UNIGRID Battery, San Diego, California 92121, United States

⁴Sustainable Power and Energy Center, University of California, San Diego, La Jolla, California 92093, United States

=These authors contributed equally to this work.

^zE-mail: zhc199@ucsd.edu

Abstract

Tin (Sn) is a promising anode material for sodium-ion batteries (SIBs) due to its high theoretical specific capacity (847 mAh g⁻¹) and volumetric capacity (6238 mAh cm⁻³). In addition, Sn is a commodity and can be readily sourced. However, alloy anodes tend to suffer from a low initial Coulombic efficiency (ICE) and severe capacity loss due to extensive volume expansion (~420% for Sn) during electrochemical cycling. In this work, commodity-sourced Sn is used (with an electrode active material composition of >99% Sn) to demonstrate how these traditional challenges can be overcome without major modifications. When paired with a NaCrO₂ (NCrO) cathode in a full cell, a high specific energy of 178 Wh/kg and volumetric energy density of 417 Wh/L can be achieved. This work highlights the opportunities for alloy materials such as Sn to enable high energy density SIBs.

Introduction

Recent challenges in geopolitics and supply chain constraints have driven interest in alternatives to lithium-ion technologies, especially for energy storage applications such as electric mobility and stationary storage. One such alternative is sodium-ion batteries (SIBs), which has the potential to eliminate the use of critical materials such as lithium (Li), nickel (Ni), cobalt (Co) and copper (Cu) in its production; typically, the supply chain for these critical materials have been limited to

a few regions in the world.^{1, 2} Additionally, SIBs offer the opportunity to utilize commodity-scale precursor materials, meaning, tapping into established supply chains without requiring large capital investments into new infrastructure.³ Electrochemically, SIBs are well-known to be able to operate effectively over a wider temperature range and can be far safer than lithium-ion batteries (LIBs).⁴ Despite these advantages, SIBs are often criticized for having a lower energy density compared to LIBs.⁵ To overcome this, alloy anodes directly address this issue.

Conventionally, hard carbon (HC) has been the anode of choice in SIBs. Its properties (typical specific capacity around 300 mAh g⁻¹, and a calendared density of 0.9 g cm⁻³) means that HC is a limiting factor for the energy density for SIBs (Figure 1a).^{6,7} In contrast, alloy materials such as tin (Sn) have a much higher specific capacity (~847 mAh g⁻¹) and volumetric capacity (6238 mAh cm⁻³, and a calendared density of 7.3 g cm⁻³) through the formation of dense Na-Sn alloys.⁸ An anode with such characteristics would increase both the gravimetric and volumetric energy density of SIBs (Figure 1b). Moreover, the denser structure of Sn facilitates the design of high-loading electrodes, which can significantly lower the production costs of SIBs by reducing the energy requirements involved in solvent usage and the drying thereof, while also increasing overall throughput.

Sn-based anodes are not new to the battery field; they have been explored in LIBs alongside silicon for the same motivation, to improve upon the energy density limitations of graphite. However, Sn has not been successful in LIBs, with issues such as a low initial Coulombic efficiency (ICE) and poor cycling stability. This is primarily due to severe volumetric expansion during cycling among other reasons. To address these challenges, considerable research has focused on a myriad of strategies, such as: particle size control to achieve nanoscale target morphologies, developing Sn-carbon nanocomposites with engineered structures, the use of various binders and carbon additives, the use of pre-lithiation or partial oxidation strategies, and the use of electrolyte additives and specialized salts to improve the interfaces. However, an effective solution remains elusive.

In this work, we propose to directly utilize the intrinsic, favorable properties of commodity-scale Sn (325 mesh, Figure S1) to address the mentioned challenges. To do so, three critical assumptions are made: 1) Since Sn is intrinsically electronically conductive, significant amounts of binders or carbon additives for electrode preparation are not necessary, 2) Sn is intrinsically compliant under mild stack pressure, and 3) Sn operates in a less reductive environment compared to LIBs, 0.005 – 0.4 V vs Na/Na⁺, (equivalent to 0.335 – 0.73 V vs Li/Li⁺), and thus experiences significantly less electrolyte reduction. With these three assumptions, it becomes clear that previous strategies applied in the literature may not be effective in addressing the root causes of Sn's challenges. This work seeks to show that Sn can be used with minimal modifications and that Sn can achieve reversible operation during alloying and de-alloying without the need for complicated strategies.

Experimental

Preparation of Sn-based electrodes

The Sn powder (Atlantic Tin) was provided by UNIGRID Inc. The Sn anode composition used is a modified version of previous work, ²⁰ which used 79.5% Tin, 9.4% carbon black, 0.5% SWCNT, 9.9% PAANa, and 0.7% CMC. In this work, we increased the Tin % to 99.5%, with the remaining 0.25% SWCNT, 0.25% CMC for viscosity control, with the goal to eliminate the bulky carbon black and PAANa binder. The slurry was directly cast under ambient conditions on a 12μm-thick Al current collector using a transfer coater under the lowest thickness setting. Due to the high density of the >99% Sn electrode, the casting speed was optimized to achieve the target mass loading. The same process was repeated on the reverse side of the Al current collector. The dried electrode spool was then calendared using stainless steel rollers until the final target thickness was achieved.

Preparation of NaCrO2 electrodes

The NCrO powder was provided by UNIGRID Inc. and used directly. The NCrO powder was mixed with super P (SP) and PVDF in a N-Methyl-2-Pyrrolidone (NMP) solution with a final composition of 96.9:2.1:1 (NCrO:SP:PVDF). The NCrO electrode was cast on a $12\mu m$ -thick Al current collector using a transfer coater in a humidity-controlled environment (dew point <-30°C). The thickness gap of the transfer coater was adjusted until the target loading was achieved. The dried electrode spool was then calendared using stainless steel rollers until the final target electrode density of 3 g cm⁻³ is achieved.

Characterization

Scanning electron microscopy (SEM) images were obtained using FEI Apreo SEM with an electron beam setting of 5 kV and 0.1 nA. EIS was measured at open-circuit, and a frequency range from 1 MHz to 0.1 Hz with an amplitude of 5 mV was used, on a Biologic VSP-300.

The FEI Scios DualBeam FIB/SEM system was used to obtain the cross-sectional images of the Sn electrodes. Liquid N₂ was used to cool down the sample stage to -180°C to create a cryogenic environment which minimizes beam damage to the sample. The FIB/SEM uses a gallium ion beam, and a voltage of 30 kV, current of 7 nA and dwell time of 100 ns was used to roughly mill down the cross-section of the deposited lithium. After the rough milling, the cross-section is cleaned with the ion beam at a current of 1 nA. The SEM image of the cross-section was taken using the Everhart-Thornley Detector (ETD) at 5 kV and 0.1 nA.

Electrochemical performance

Direct current polarization (DCP) was performed on Sn powder that was pelletized at 100 MPa using a hydraulic press. Applied voltages ranged from 0.05 V to 0.2 V, and the corresponding response currents were used to determine the electronic conductivity based on Ohm's law.

For electrochemical data, coin type (CR2032) cells were assembled inside an argon-filled glove box. The half cells were assembled with the Sn working electrode, glass fiber separator (GF/F), sodium chip as a counter electrode, stainless-steel spacer, and stainless-steel disc spring, Each half cell contained 100 µL of 1 M NaFSI salt in DME and full cell contained 100 µL of the electrolyte. Cells were rested for 8 hours after crimping and cycled between 0.005 and 1.0 V vs. Na⁺/Na on a Neware Battery Testing System.

The Sn-NCrO pouch cells were assembled in humidity-controlled (dew point <-30°C) dry room. The detailed parameters of the pouch cells were summarized in Table 1. 36 pieces of Sn electrodes and 35 pieces of NCrO electrodes were assembled in the Z-stack configuration. The pouch cell was then dried under vacuum at 80°C for 24 hours before electrolyte injection. Each pouch cell is injected with 40g (E/C ratio ~2.35) of 1 M NaFSI salt in DME electrolyte. The Sn-NCrO pouch cells were formed by conducting a charge and discharge cycle, then degassed under vacuum. Subsequently, the Sn-NCrO pouch cells are cycled at room temperature with pressure plates held together by bolts and nuts tightened to apply stack pressure using a torque wrench with 20 Nm of applied torque.

Results

Electrode fabrication and characterization

To evaluate the three critical assumptions, characterization was done on commodity-sourced Sn powder. A direct current polarization measurement (DCP, Figure S2) found that Sn powder has an electronic conductivity of 6.7x10⁴ S cm⁻¹, a sufficiently high value to conduct electrons even without carbon additives. This conductivity is also several orders of magnitude higher than most anode active materials (10⁻⁶-10³ S cm⁻¹).²¹⁻²⁵ Comparatively, silicon, a semiconductor, has a reported electronic conductivity of 2.5x10⁻⁴ S cm⁻¹, eight orders of magnitude lower than Sn.²⁵ Therefore, significant amounts of carbon additives are needed with silicon (in LIBs), but not with Sn. Figure 1c shows the anode slurry (water-based), containing >99% Sn active material, cast on an Al current collector. Figure 1d shows the punched and calendared Sn electrodes, which are gray in color due to the high active material (>99% Sn) in the electrode.

To evaluate the hardness of Sn powders, a tap density measurement was conducted using a pellet die setup. When 100 MPa of pressure was applied to Sn powder, the measured density was 7.3 g cm⁻³, which matches to the theoretical density of metallic Sn.²⁶ Comparatively, pressed Si has a measured density of 1.38 g cm⁻³, significantly lower than the theoretical density of metallic Si (2.33 g cm⁻³).^{27, 28} These results correspond well to the literature, as the reported yield strengths of Sn and Si are 7.7 MPa and 7000 MPa, respectively.^{29, 30} Given that alloys will further soften as they get sodiated, the yield strength of Na-Sn is expected to be even lower, and any volume change in the Z-axis of the Sn electrode can now be easily suppressed with a small amount of applied stack pressure.

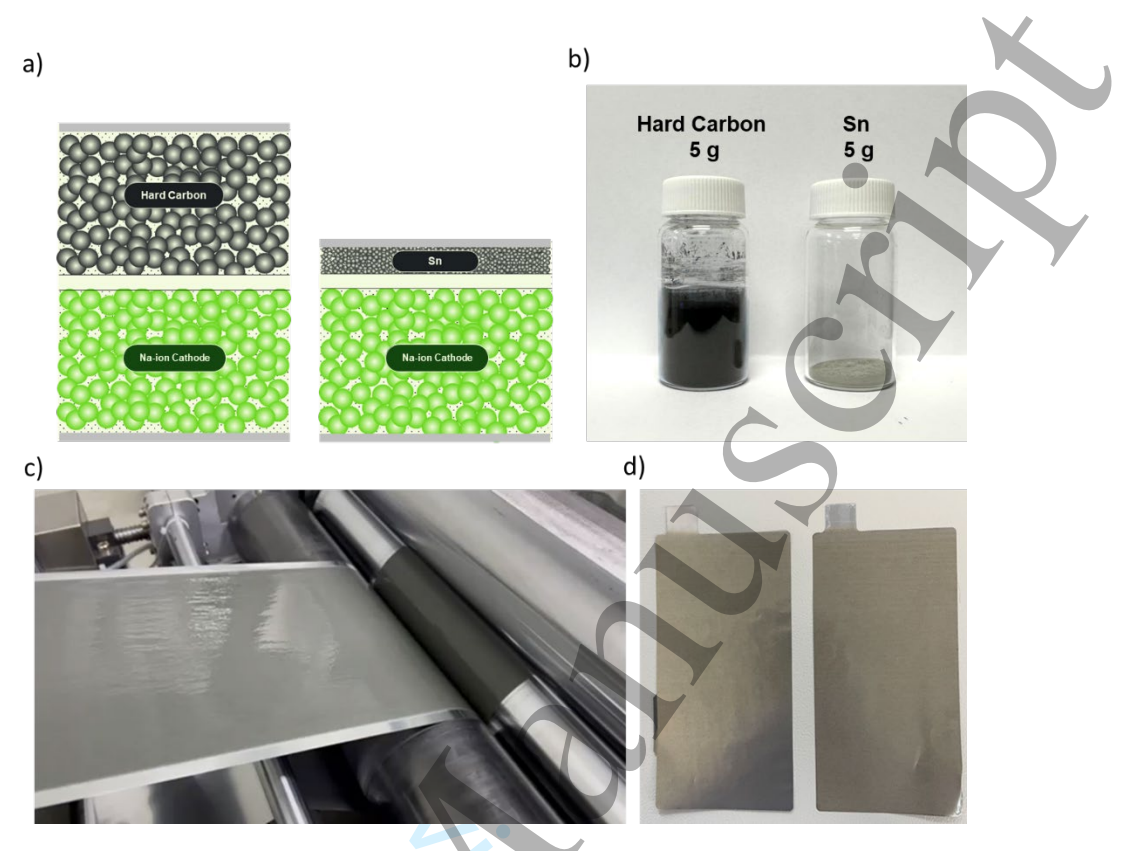


Figure 1. (a) Schematics of cell thickness comparison between hard carbon-based Na-ion cell and Sn-based Na-ion cell. Digital images of (b) 5g of hard carbon and Sn powders, (c) Sn slurry cast on an Al current collector (d) Punched and calendared Sn electrodes from the dried cast.

The nominal electrochemical potential of Sn with respect to Na/Na⁺ can be verified in a half cell. From Figure 2a, the operating potential of Sn during sodiation is 0.005 - 0.4 V vs. Na/ Na⁺, which corresponds to 0.335 - 0.73 V vs. Li/Li⁺. Due to a 0.33 V higher operating potential, the organic electrolyte is exposed to a relatively milder reductive environment in SIB anodes. While this does not entirely prevent electrolyte reduction and SEI formation, it may still mitigate excessive SEI accumulation during cycling compared to lithium systems. Furthermore, ether-based electrolytes are reported to form thinner and more stable SEI layers compared to carbonate-based electrolytes in Sn and HC anodes. ^{26, 31} These result in highly reversible kinetics of sodiation and de-sodiation, evidenced by the overlapping voltage curves of the half cell.

Interestingly, the 1st cycle Coulombic efficiency was 89.35% with a de-sodiation capacity of 731.8 mAh g⁻¹. In subsequent cycles, the de-sodiation capacity increased and remained stable at approximately 800 mAh g⁻¹. It is hypothesized that the micron-sized Sn particle needs to undergo an activation process during cycling and then reach equilibrium. This phenomenon was also reported in previous work, where structural re-ordering of alloy particles results in higher surface area for improved Na⁺ transport properties (Figure 2d-f).^{20, 32} Such an effect is also supported by Figure 2b, where a significant drop in cell impedance is observed between cycle 1 to cycle 20

(Table S1), indicative of an activation process that improves the transport kinetics of the Na-Sn alloy.

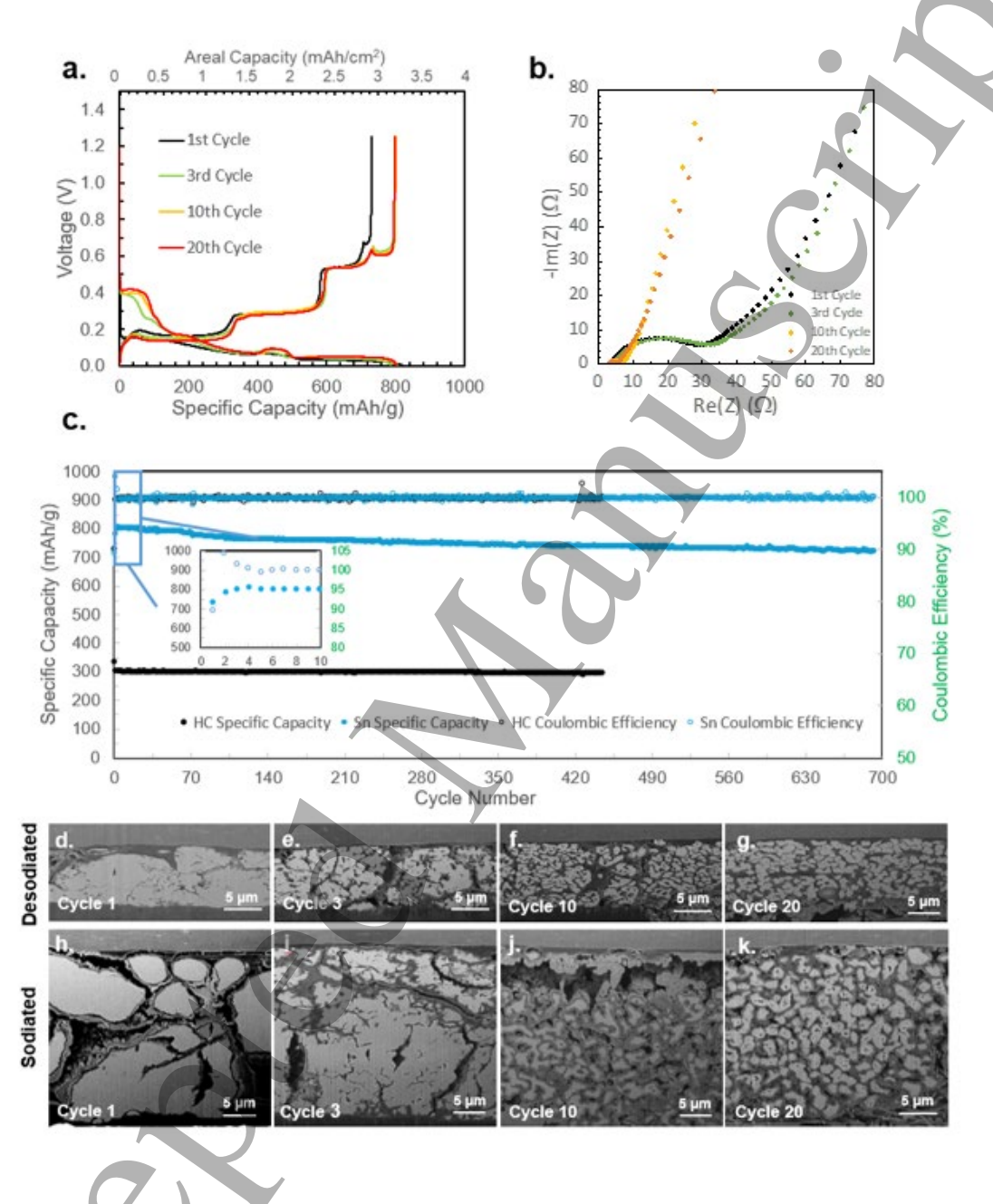


Figure 2. Electrochemical properties of Sn tested in a half cell vs Na/Na⁺. (a) Voltage profile of the 1st, 3rd, 10th and 20th cycle, (b) Nyquist plots of the half cell at the 1st, 3rd, 10th and 20th cycle, (c) Extended cycle life and Coulombic efficiency plots of the Sn electrode compared with a HC electrode. FIB-SEM cross-sectional images of the desodiated Sn electrode after (d-g) 1, 3, 10, and 20 cycles, and the sodiated Sn electrode after (h-k) 1, 3, 10, and 20 cycles, respectively.

Figure 2c shows the cycle life of the Sn electrodes compared to hard carbon. While some fluctuations are seen in the first 100 cycles, likely due to Sn's initial volume changes occurring during cycling that affect interparticle contact, the overall capacity retention remains comparable to hard carbon. As the half-cell is operated in a coin cell without any external stack pressure, this fluctuation is expected to take longer to equilibrate. To visualize this structural evolution during Sn particle activation, cross sectional images were taken with a focused ion beam scanning electron microscope (FIB-SEM). In Figure 2d-f, the Sn particles undergo structural and morphological changes during the initial cycling, which corresponds to what previous work has reported.^{33, 34} At cycle 1, distinct microparticles can be seen. As cycling proceeds, the micro-structure of the particles appears to transform from large, discreet particles to a network of smaller, interconnected particles. Despite this, the average Coulombic efficiencies for the Sn electrodes and hard carbon are 99.93% and 99.95%, respectively, demonstrating the high reversibility of commodity-sourced Sn powders in the absence of excessive amounts of binders or additives.

Full cell assembly and electrochemical data

To evaluate the Sn electrode in a full cell, the NaCrO₂ (Figure S3) cathode is chosen as a counter electrode due to its well established stability and high capacity in SIB.³⁵⁻³⁷ Both electrodes were prepared and fabricated into a pouch cell. The detailed design specifications of the full pouch cell are found in Table 1.

Table 1. Design sheet of the full Sn | NaCrO₂ pouch cell.

Cathode	Capacity (mAh g ⁻¹)	120
	Active Material (AM) ratio (%)	96.9
	Thickness (double layer + 12μm Al foil, μm)	132
	Areal capacity (mAh cm ⁻²)	2
Separator	Thickness (μm)	16
Anode	Capacity (mAh g ⁻¹)	800
	Active Material (AM) ratio (%)	99.5
	Thickness (double layer + 12μm Al foil, μm)	25
	Areal capacity (mAh cm ⁻²)	2.1
Current Collector	Al for cathode (μm)	12
	Al for anode (μm)	12
Dimensions	L x W (mm)	$175 \times 80 \pm 0.2$
Layers	Anode/Cathode	36/35

Pouch bag	Thickness (mm)	0.12 x 2
Total thickness (Charged)	Thickness (mm)	8.0 ± 0.1
Total mass	Mass (g)	262 ± 5
Nominal Voltage (V)	2.75	YY
Nominal Capacity (Ah)	17.0	
Specific Energy (Wh kg ⁻¹)	178 Wh kg ⁻¹	,
Volumetric Energy (Wh L-1)	417 Wh L ⁻¹	
	Cell Pictures	
2 4 5 6 7 8	9 9 10 11 52 9 10 11 5	

This pouch cell achieves a reversible capacity of 17.0 Ah and a nominal voltage of 2.75 V (when cycled between 2.2 V to 3.4 V; voltage curve in Figure 4a). The pouch cell has a total mass of 0.262 kg and a volume of 0.112 L at the fully charged state, yielding a specific energy of 178 Wh kg⁻¹ and volumetric energy density of 417 Wh L⁻¹.

To evaluate the impedance growth of the Sn | NaCrO₂ full cell with cycle numbers, Figure 4b shows the EIS measurements of the pouch cell at the discharged state at cycles 1, 3, 10, and 20 respectively. Similar to what was observed in the half cell, the pouch cell impedance was observed to decrease after the first cycle, from $2.27 \cdot 10^{-2} \Omega$ after 1 cycle to $2.04 \cdot 10^{-2} \Omega$ after 3 cycles, to $1.60 \cdot 10^{-2} \Omega$ after 10 cycles and finally $1.42 \cdot 10^{-2} \Omega$ after 20 cycles. This corresponds to the same activation effect of the Sn particles previously reported in the literature and in Figure 2b.²⁰

To assess the rate capability of pouch-type sodium-ion cells, systematic charge and discharge rate tests were conducted (Figure 4c, Figure S4). In the charge rate evaluation, the charging current was varied while maintaining a constant discharge rate of C/10. For the discharge rate assessment, the discharge current was varied while the charging rate was fixed. The maximum current applied

during these tests was 8 A (corresponding to C/2). The discharge rate test was subsequently performed following completion of the charge rate test using the same cell. The charge capacity exhibited a minimal reduction of approximately 1% when the rate increased from C/10 (charge capacity of Cycle 3) to C/2 (charge capacity of Cycle 12). In contrast, the discharge capacity declined by approximately 5% over the same rate increase, from C/10 (discharge capacity of Cycle 15) to C/2 (discharge capacity of Cycle 24). These results indicate that the desodiation kinetics of Sn at higher rates are slower compared to the sodiation process, suggesting a rate-limiting behavior during sodium extraction.



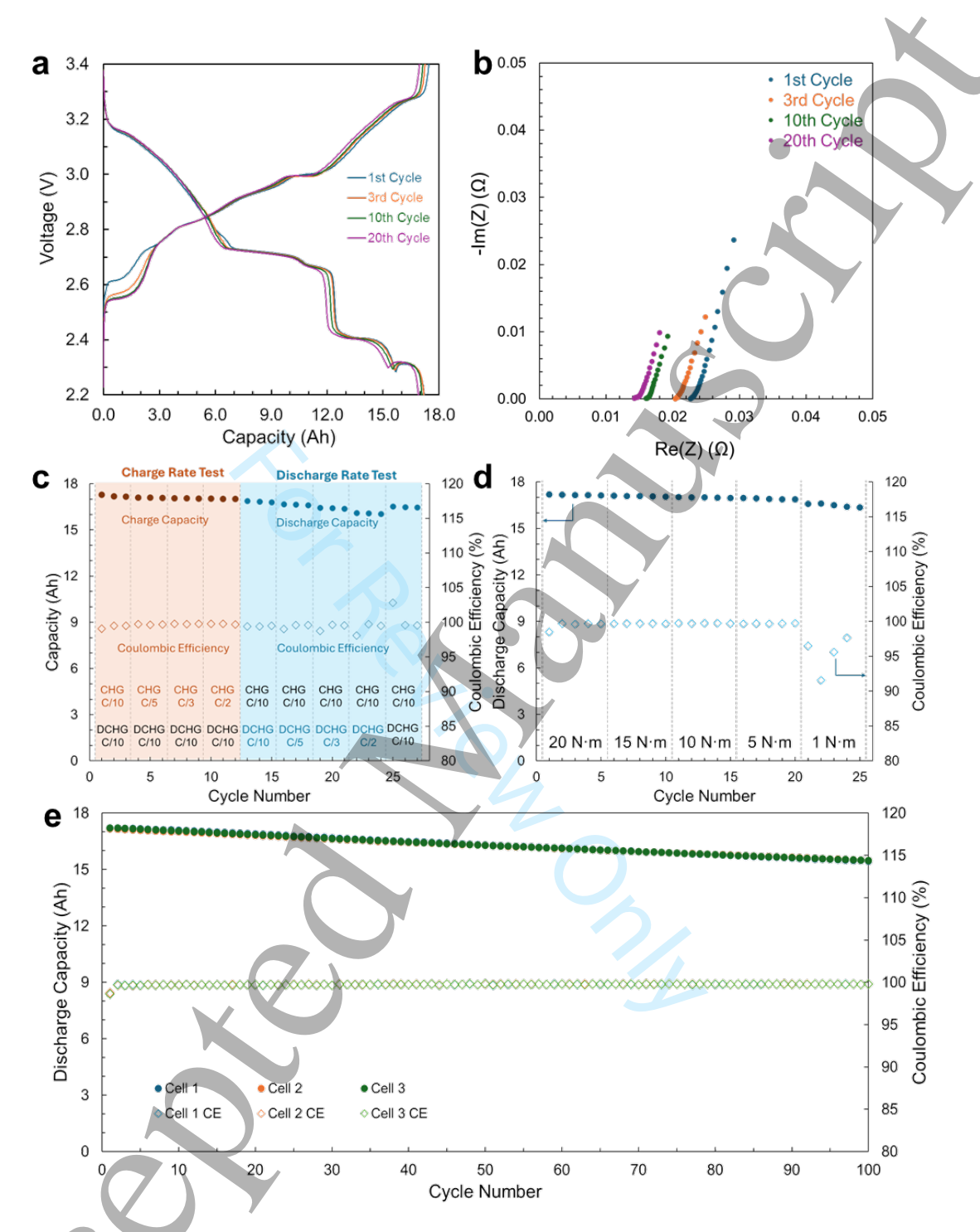


Figure 4. (a) Voltage curves of the Sn | NaCrO₂ pouch full cell. (b) Nyquist plot showing the EIS measurements of the full cell after cycles 1, 3, 10, and 20. (c) Charge and discharge rate test. (d) Discharge capacity and Coulombic efficiency with the cell stacking plate tightened at different torques. (e) Cycle life and Coulombic efficiency plots of the pouch cells.

To evaluate the effect of stack pressure on the pouch cell, a pouch cell was sandwiched between stainless steel pressure plates. The bolts were tightened with a torque value of 20 Nm, and the cells were then cycled at a rate of C/5 at room temperature (Figure S5) for 5 cycles. Subsequently, the

test was repeated at 15 Nm, 10 Nm, 5 Nm and 1 Nm, to evaluate the effect on reversible capacity and Coulombic efficiency with respect to torque (Figure 4d, Figure S6). The discharge capacity remained relatively stable from 20 Nm down to 5 Nm. Below 5 Nm, however, a decrease of approximately 5% in discharge capacity was observed compared to the initial value recorded at 20 Nm. It is noteworthy that a torque of 1 Nm, which is equivalent to hand-tightening, was sufficient to maintain functional operation of the Sn pouch cell. This suggests that a high external pressure is not critical for the electrochemical cycling and operation of the cells in this study.

To evaluate the cycle life, three pouch cells were sandwiched between stainless steel pressure plates, the bolts were tightened at 20 Nm, and the cells were cycled at a rate of C/5 at room temperature. All three cells showed an average capacity retention of 90.0% after 100 cycles, with an average Coulombic efficiency of 99.7%.

Discussion

Among various next-generation battery technologies, SIBs have undoubtedly made rapid progress toward commercialization in recent years, with numerous cell products now commercially available. Figure 5 is a summary of the SIB landscape as reported by the Volta Foundation's Battery Report 2024, containing publicly-available cell datasheets from commercial products. When plotted by specific energy versus volumetric energy density, it is interesting to see two major clusters appear, based on chemistry. One cluster is the polyanion-based chemistry, such as the Na₃V₂(PO₄)₃, Na₃V₂(PO₄)₂F₃, or Na₄Fe₃(PO₄)₂(P₂O₇) cathodes paired with hard carbon, and the second is the layered oxide type chemistry, such as the Na_{Nix}Fe_yMn_zO₂, Na₂Cu_xFe_yMn_zO₂ or Na₄Fe_xMn_yO₂ cathodes paired with hard carbon. ³⁹⁻⁴⁴ While it is no surprise that the polyanion cathodes have significantly lower energy density than layered oxides, both types of SIBs, if they use hard carbon anodes, will have much lower energy densities than the state-of-the-art Li-ion LFP. This is evident when volumetric energy density (Wh L⁻¹) is considered, a metric often unreported and overlooked.

Considering the emerging applications in micro-mobility or low speed vehicles, stationary storage, and distributed energy applications, volumetric energy is arguably more relevant for consideration than specific energy.⁴⁵ Advancements in cathode innovation have brought incremental improvements in the energy densities of SIBs, but it has become clear that the hard carbon anode is the prevailing bottleneck to higher energy densities, especially in applications where volume, or deployment footprint is crucial. Energy-dense alloy anodes are thus necessary to overcome the hard carbon bottleneck to significantly increase volumetric energy densities for SIBs.

Although energy-dense alloy anodes have faced formidable challenges when used in Li-ion batteries, such as silicon, these barriers can be overcome in SIBs without using costly materials or complicated techniques. This work has demonstrated a proof-of-concept that using commodity-sourced Sn metal powders as the anode allows SIBs to achieve both higher specific energy density and volumetric energy density compared to the state-of-the-art LFP.

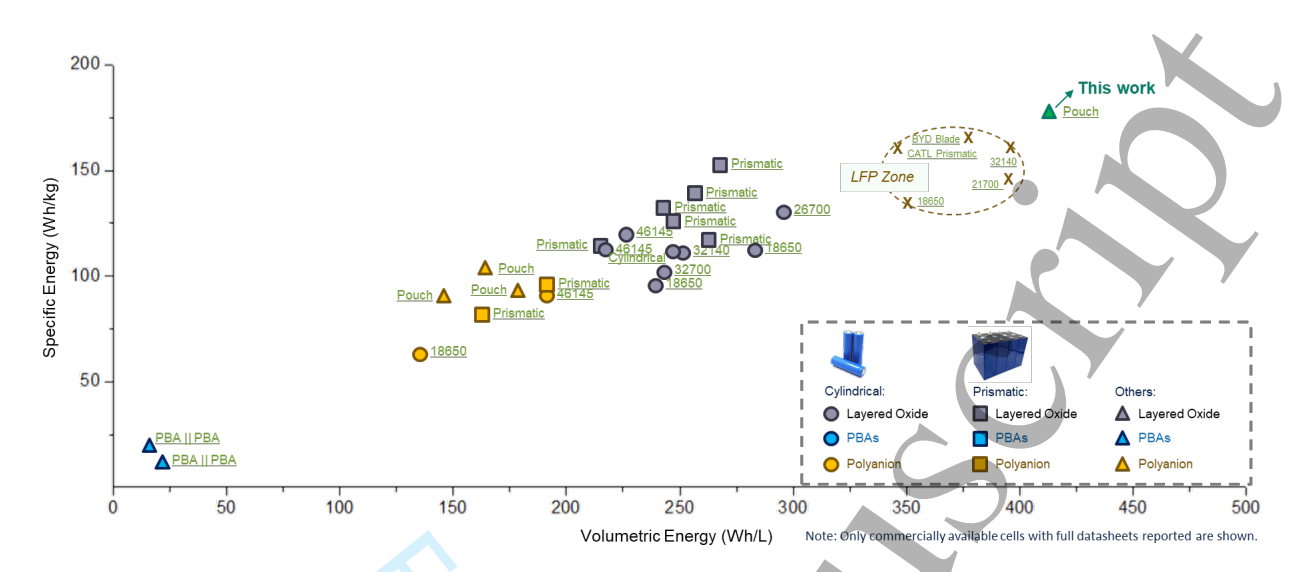


Figure 5. Specific Energy (Wh/kg) vs Volumetric energy density (Wh/L) comparison of commercially-reported SIBs based on public datasheets, along with reference LIB (LFP) datapoints. 38, 46-50

Despite the unprecedented energy densities achieved in the pouch cell, the overall performance of the Sn-NaCrO₂ cell can still be improved with further work. Specifically, the cycle life of the pouch cell, achieving 100 cycles with 90.0% retention, needs to improve to be viable in most commercial applications. The cell design used in this work serves as a proof-of-concept to illustrate the capabilities of alloy materials such as Sn when used in its barest form without any complex electrode or electrolyte modifications. Further optimization in future work through strategies such as electrode additive screening, electrolyte modifications, and structural or mechanical design changes can be conducted to improve the rate capability, reduce the dependence on stack pressure and extend cycle life significantly.⁵¹⁻⁵³

Conclusion

This work aimed to show that commodity-sourced Sn, when processed in an electrode (>99% active Sn) and used in a SIB, could achieve high specific energy, high volumetric energy density, and reversible operation without the need for costly and complex nanoscale material processing or techniques. This is achievable due to the intrinsic properties of Sn which are markedly different than the intrinsic properties of Si. Notably, Sn is intrinsically electronically conductive (eight orders of magnitude higher than Si), so an excessive amount of binder or carbon additives are not necessary to make a functioning electrode. Sn is intrinsically mechanically soft and compliant under mild stack pressure, which mitigates the effects of volume expansion, and Sn operates in a less reductive environment, 0.2 V vs Na/Na⁺, equivalent to 0.5 V vs Li/Li⁺, and thus experiences significantly less electrolyte reduction. This study culminated in the fabrication of a 17 Ah SIB, a pouch-format full cell, containing Sn as the anode and NaCrO₂, a layered oxide, as the cathode. A specific energy of 178 Wh kg⁻¹ and volumetric energy density of 417 Wh L⁻¹ were achieved,

exceeding the values of the state-of-the-art Li-ion LFP. Alloy anodes are thus demonstrated as a viable route for high-performance, energy dense SIBs that directly address the energy density criticism when compared against LIBs.

Acknowledgement

This work is partially supported by the start-up funding from UC San Diego (Z.C.)

Author Contributions

Conceptualization, Z.C. W. T., D. T., Methodology, S. K., W. T., D. T., E. W., Formal Analysis, Z. C., S. K., W. T., D. T., E. W., B. L., Investigation, S.K., W. T., B. L., E. W., Resources, Z. C., D. T., Writing—Original Draft, S. K., W. T., Writing—Review & Editing, Z. C., S. K., W. T., D. T., E. W., B. L., Funding Acquisition, Z. C., Supervision, Z. C., S. K. and W. T. contributed equally to this work.

Declaration of Interests

Z.C. is a co-founder and equity share holder of Unigrid Battery.

References

- 1. Yao, A.; Benson, S. M.; Chueh, W. C., Critically assessing sodium-ion technology roadmaps and scenarios for techno-economic competitiveness against lithium-ion batteries. *Nature Energy* **2025**, *10* (3), 404-416.
- 2. Podobińska-Staniec, M.; Wiktor-Sułkowska, A.; Kustra, A.; Lorenc-Szot, S., Copper as a Critical Resource in the Energy Transition. *Energies* **2025**, *18* (4), 969.
- 3. Duffner, F.; Kronemeyer, N.; Tübke, J.; Leker, J.; Winter, M.; Schmuch, R., Post-lithium-ion battery cell production and its compatibility with lithium-ion cell production infrastructure. *Nature Energy* **2021**, 6 (2), 123-134.
- 4. Carter, R.; Waller, G. H.; Jacob, C.; Hayman, D.; West, P. J.; Love, C. T., First Look at Safety and Performance Evaluation of Commercial Sodium-Ion Batteries. *Energies* **2025**, *18* (3), 661.
- 5. Tarascon, J.-M., Na-ion versus Li-ion Batteries: Complementarity Rather than Competitiveness. *Joule* **2020**, *4* (8), 1616-1620.
- 6. Constable, C.; Coowar, F.; Copley, M.; Kendrick, E.; Dancer, C.; Hasa, I., Influence of Particle Size and Mass Loading of Hard Carbon on Sodium Ion Battery Rate Performance in Industrially Relevant Full Cells. *Journal of The Electrochemical Society* **2024,** *171* (2), 023506.
- 7. Stevens, D. A.; Dahn, J. R., High Capacity Anode Materials for Rechargeable Sodium-Ion Batteries. *Journal of The Electrochemical Society* **2000**, *147* (4), 1271.

- 8. Ma, W.; Yin, K.; Gao, H.; Niu, J.; Peng, Z.; Zhang, Z., Alloying boosting superior sodium storage performance in nanoporous tin-antimony alloy anode for sodium ion batteries. *Nano Energy* **2018**, *54*, 349-359.
- 9. Ying, H.; Han, W.-Q., Metallic Sn-Based Anode Materials: Application in High-Performance Lithium-Ion and Sodium-Ion Batteries. *Advanced Science* **2017**, *4* (11), 1700298.
- 10. Todd, A. D. W.; Ferguson, P. P.; Fleischauer, M. D.; Dahn, J. R., Tin-based materials as negative electrodes for Li-ion batteries: Combinatorial approaches and mechanical methods. *International Journal of Energy Research* **2010**, *34* (6), 535-555.
- 11. Hassoun, J.; Derrien, G.; Panero, S.; Scrosati, B., A Nanostructured Sn–C Composite Lithium Battery Electrode with Unique Stability and High Electrochemical Performance. *Advanced Materials* **2008**, *20* (16), 3169-3175.
- 12. Cook, J. B.; Lin, T. C.; Detsi, E.; Weker, J. N.; Tolbert, S. H., Using X-ray Microscopy To Understand How Nanoporous Materials Can Be Used To Reduce the Large Volume Change in Alloy Anodes. *Nano Letters* **2017**, *17* (2), 870-877.
- 13. Xu, H.; Li, S.; Chen, X.; Zhang, C.; Liu, W.; Fan, H.; Yu, Y.; Huang, Y.; Li, J., Sn-Alloy Foil Electrode with Mechanical Prelithiation: Full-Cell Performance up to 200 Cycles. *Advanced Energy Materials* **2019**, 9 (42), 1902150.
- 14. Zhang, N.; Sun, C.; Huang, Y.; Zhu, C.; Wu, Z.; Lv, L.; Zhou, X.; Wang, X.; Xiao, X.; Fan, X.; Chen, L., Tuning electrolyte enables microsized Sn as an advanced anode for Li-ion batteries. *Journal of Materials Chemistry A* **2021**, 9 (3), 1812-1821.
- 15. Liu, H.; Wang, S.; Zhao, J.; Zhang, B.; Liu, L.; Bao, R.; Jing, Z., Sn-based anode materials for lithium-ion batteries: From mechanism to modification. *Journal of Energy Storage* **2024**, *80*, 109862.
- 16. Liu, H.; Wang, S.; Liu, L.; Zhao, J.; Zhang, W.; Bao, R.; Wang, L.; Yang, J.; Li, Y.; Jing, Z., Strategies, perspectives, and challenges of improving the initial coulombic efficiency and tap density of Sn-based anode materials for lithium-ion batteries. *Chemical Engineering Journal* **2024**, *495*, 152444.
- 17. Wu, X.; Lan, X.; Hu, R.; Yao, Y.; Yu, Y.; Zhu, M., Tin-Based Anode Materials for Stable Sodium Storage: Progress and Perspective. *Advanced Materials* **2022**, *34* (7), 2106895.
- 18. Shen, H.; An, Y.; Man, Q.; Liu, D.; Zhang, X.; Ni, Z.; Dai, Y.; Dong, M.; Xiong, S.; Feng, J., Chemical Prelithiation/Presodiation Strategies Toward Controllable and Scalable Synthesis of Microsized Nanoporous Tin at Room Temperature for High-Energy Sodium-Ion Batteries. *Advanced Functional Materials* **2024**, *34* (7), 2309834.
- 19. Chu, C.; Zhou, L.; Cheng, Y.; Wang, X.; Chang, L.; Nie, P.; Wang, C.; Wang, L., Ultralow-Concentration (0.1M) Electrolyte for stable bulk alloy (Sn, Bi) anode in Sodium-ion battery via Regulating Anions Structure. *Chemical Engineering Journal* **2024**, *482*, 148915.
- 20. Garayt, M. D. L.; Zhang, Y.; Obialor, M. C.; Deshmukh, J.; Xing, Y.; Yang, C.; Metzger, M.; Dahn, J. R., Practical Alloy-Based Negative Electrodes for Na-ion Batteries. *Journal of The Electrochemical Society* **2024**, *171* (7), 070523.
- 21. Wen, Y.; He, K.; Zhu, Y.; Han, F.; Xu, Y.; Matsuda, I.; Ishii, Y.; Cumings, J.; Wang, C., Expanded graphite as superior anode for sodium-ion batteries. *Nature Communications* **2014**, *5* (1), 4033.

- 22. Yang, W.; Yang, W.; Ding, F.; Sang, L.; Ma, Z.; Shao, G., Template-free synthesis of ultrathin porous carbon shell with excellent conductivity for high-rate supercapacitors. *Carbon* **2017**, *111*, 419-427.
- 23. Yu, Z.-L.; Xin, S.; You, Y.; Yu, L.; Lin, Y.; Xu, D.-W.; Qiao, C.; Huang, Z.+H.; Yang, N.; Yu, S.-H.; Goodenough, J. B., Ion-Catalyzed Synthesis of Microporous Hard Carbon Embedded with Expanded Nanographite for Enhanced Lithium/Sodium Storage. *Journal of the American Chemical Society* **2016**, *138* (45), 14915-14922.
- 24. Yan, W.; Mu, Z.; Wang, Z.; Huang, Y.; Wu, D.; Lu, P.; Lu, J.; Xu, J.; Wu, Y.; Ma, T.; Yang, M.; Zhu, X.; Xia, Y.; Shi, S.; Chen, L.; Li, H.; Wu, F., Hard-carbon-stabilized Li–Si anodes for high-performance all-solid-state Li-ion batteries. *Nature Energy* **2023**, *8* (8), 800-813.
- 25. Ham, S.-Y.; Sebti, E.; Cronk, A.; Pennebaker, T.; Deysher, G.; Chen, Y.-T.; Oh, J. A. S.; Lee, J. B.; Song, M. S.; Ridley, P.; Tan, D. H. S.; Clément, R. J.; Jang, J.; Meng, Y. S., Overcoming low initial coulombic efficiencies of Si anodes through prelithiation in all-solid-state batteries. *Nature Communications* **2024**, *15* (1), 2991.
- 26. Zhang, B.; Rousse, G.; Foix, D.; Dugas, R.; Corte, D. A. D.; Tarascon, J.-M., Microsized Sn as Advanced Anodes in Glyme-Based Electrolyte for Na-Ion Batteries. *Advanced Materials* **2016**, *28* (44), 9824-9830.
- 27. Lin, D.; Lu, Z.; Hsu, P.-C.; Lee, H. R.; Liu, N.; Zhao, J.; Wang, H.; Liu, C.; Cui, Y., A high tap density secondary silicon particle anode fabricated by scalable mechanical pressing for lithium-ion batteries. *Energy & Environmental Science* **2015**, 8 (8), 2371-2376.
- 28. Jin, Y.; Zhu, B.; Lu, Z.; Liu, N.; Zhu, J., Challenges and Recent Progress in the Development of Si Anodes for Lithium-Ion Battery. *Advanced Energy Materials* **2017**, *7* (23), 1700715.
- 29. Zhang, H.; Ma, Z.; Yang, S.; Fan, M.; Cheng, X., Microstructure and mechanical properties of Sn-xGa alloys and solder joints. *Journal of Materials Research and Technology* **2023**, *26*, 3830-3839.
- 30. Canham, L., Mechanical Properties of Porous Silicon. In *Handbook of Porous Silicon*, Canham, L., Ed. Springer International Publishing: Cham, 2018; pp 309-318.
- 31. Yin, X.; Wang, Z.; Liu, Y.; Lu, Z.; Long, H.; Liu, T.; Zhang, J.; Zhao, Y., Insight into the influence of ether and ester electrolytes on the sodium-ion transportation kinetics for hard carbon. *Nano Research* **2023**, *16* (8), 10922-10930.
- 32. Kim, C.; Kim, H.; Sadan, M. K.; Jeon, M.; Cho, G.; Ahn, J.; Kim, K.; Cho, K.; Ahn, H., Development and Evaluation of Sn Foil Anode for Sodium-Ion Batteries. *Small* **2021**, *17* (50), 2102618.
- 33. Kim, C.; Kim, I.; Kim, H.; Sadan, M. K.; Yeo, H.; Cho, G.; Ahn, J.; Ahn, J.; Ahn, H., A self-healing Sn anode with an ultra-long cycle life for sodium-ion batteries. *Journal of Materials Chemistry A* **2018**, 6 (45), 22809-22818.
- 34. Garayt, M. D. L.; Obialor, M. C.; Monchesky, I. L.; George, A. E.; Yu, S.; Rutherford, B. A.; Metzger, M.; Dahn, J. R., Restructuring of Sodium-Lead Alloys during Charge-Discharge Cycling in Sodium-Ion Batteries. *Journal of The Electrochemical Society* **2024**, *171* (12), 120521.
- 35. Wu, J.; Tang, W.; Yang, H.; Lee, D. J.; Xu, D.; Li, F.; Qin, J.; Kim, S.; Gao, H.; Jeon, Y.; Tran, D.; Chen, Y.; Mu, A.; Bian, W.; Sun, H.; Chen, Z., Micron Size NaCrO2 Particles

Enable High-loading Dry-processed Electrode for Sodium Ion Batteries. *Small* **2025**, *21* (23), 2501504.

- 36. Chu, S.; Guo, S., From Rotten to Magical: Transition Metal Migration in Layered Sodium-Ion Battery Cathodes. *Advanced Functional Materials* **2024**, *34* (18), 2313234.
- 37. Ahangari, M.; Zhou, M.; Luo, H., Review of Layered Transition Metal Oxide Materials for Cathodes in Sodium-Ion Batteries. *Micromachines* **2025**, *16* (2), 137.
- 38. Foundation, V. Battery Report 2024; Volta Foundation, 2025; p 278.
- 39. Deng, C.; Gabriel, E.; Skinner, P.; Lee, S.; Barnes, P.; Ma, C.; Gim, J.; Lau, M. L.; Lee, E.; Xiong, H., Origins of Irreversibility in Layered NaNixFeyMnzO2 Cathode Materials for Sodium Ion Batteries. *ACS Applied Materials & Interfaces* **2020**, *12* (46), 51397-51408.
- 40. Stüble, P.; Müller, C.; Klemens, J.; Scharfer, P.; Schabel, W.; Häringer, M.; Binder, J. R.; Hofmann, A.; Smith, A., Enabling Long-term Cycling Stability of Na3V2(PO4)3/C vs. Hard Carbon Full-cells. *Batteries & Supercaps* **2024**, *7* (2), e202300375.
- 41. Yan, G.; Mariyappan, S.; Rousse, G.; Jacquet, Q.; Deschamps, M.; David, R.; Mirvaux, B.; Freeland, J. W.; Tarascon, J.-M., Higher energy and safer sodium ion batteries via an electrochemically made disordered Na3V2(PO4)2F3 material. *Nature Communications* **2019**, *10* (1), 585.
- 42. Lochab, S.; Bharathraj, S.; Mayya, K. S.; Barpanda, P.; Adiga, S. P., Unveiling the Degradation Mechanism of Sodium Ion Batteries Based on Na4Fe3(PO4)2P2O7 Cathode and Hard Carbon Anode Suggests Anode Particle Size Reduction for Cycling Stability. *Batteries & Supercaps* **2024**, *7* (8), e202400025.
- 43. Xu, J.; Chen, J.; Zhang, K.; Li, N.; Tao, L.; Wong, C.-P., Nax(Cu–Fe–Mn)O2 system as cathode materials for Na-ion batteries. *Nano Energy* **2020**, *78*, 105142.
- 44. Hirsh, H.; Olguin, M.; Chung, H.; Li, Y.; Bai, S.; Feng, D.; Wang, D.; Zhang, M.; Meng, Y. S., Meso-Structure Controlled Synthesis of Sodium Iron-Manganese Oxides Cathode for Low-Cost Na-Ion Batteries. *Journal of The Electrochemical Society* **2019**, *166* (12), A2528.
- 45. Park, K.-Y.; Lim, J.-M.; Luu, N. S.; Downing, J. R.; Wallace, S. G.; Chaney, L. E.; Yoo, H.; Hyun, W. J.; Kim, H.-U.; Hersam, M. C., Concurrently Approaching Volumetric and Specific Capacity Limits of Lithium Battery Cathodes via Conformal Pickering Emulsion Graphene Coatings. *Advanced Energy Materials* **2020**, *10* (25), 2001216.
- 46. Evlithium CATL 150 Ah LiFePO $_4$ Battery Cell. https://www.evlithium.com/catl-battery-cell/catl-150ah-lifepo4-battery-cell.html (accessed 2025, September 15).
- 47. Evlithium BYD Blade Battery 138 Ah. https://www.evlithium.com/LiFePO4-Battery/byd-blade-battery-138ah.html (accessed 2025, September 15).
- 48. Energy, S. 18650 LiFePO₄ 3.2 V 2000 mAh Rechargeable Battery for DIY 12 V/24 V/48 V Battery Pack, Flashlight, Power Bank. <a href="https://selianenergy.com/products/18650-lifepo4-3-2v-2000mah-rechargeable-battery-for-diy-12v-24v-48v-battery-pack-flashlight-power-bank?variant=44044512723177&country=US¤cy=USD&utm_medium=product_sync&utm_source=google&utm_content=sag_organic&utm_campaign=sag_organic&com_cvv=8fb3d522dc163aeadb66e08cd7450cbbdddc64c6cf2e8891f6d48747c6d56d2c (accessed 2025, September 15).

- 49. Power, W. 32140 15 Ah Cylinder LFP Cell. https://cells.welsonpower.com/products/cylinder-cells/32140-cells/32140-15ah-cylinder-lfp-cell/ (accessed 2025, September 15).
- 50. Battery, H. HAKADI 18650 3.2 V 1800 mAh LiFePO $_4$ Rechargeable Battery Cell (Cycle Life \geq 3000). https://hakadibattery.com/products/hakadi-18650-3-2v-1800mah-lifepo4-rechargeable-battery-cell-cycle-life-3000-for-diy-battery-pack-flashlight (accessed 2025, September 15).
- 51. Shen, M.; Dai, Z.; Fan, L.; Fu, H.; Geng, Y.; Guan, J.; Sun, F.; Rao, A. M.; Zhou, J.; Lu, B., Cosolvent electrolyte chemistries for high-voltage potassium-ion battery. *National Science Review* **2024**, *11* (11).
- 52. Huang, Z.-X.; Zhang, X.-L.; Zhao, X.-X.; Zhao, Y.-Y.; Aravindan, V.; Liu, Y.-H.; Geng, H.; Wu, X.-L., Electrode/electrolyte additives for practical sodium-ion batteries: a mini review. *Inorganic Chemistry Frontiers* **2023**, *10* (1), 37-48.
- 53. Li, B.; Song, J.; Zhou, J.; Chen, J.; Li, J.; Chen, J.; Wang, L.; Wu, K., Optimization of Electrode Manufacturing Processes From the Perspective of Mechanical Properties. *Journal of Electrochemical Energy Conversion and Storage* **2024**, *22* (2).

